Supplement of

Source Apportionment and Driving Mechanisms of Black Carbon in a Mountainous Megacity: Insights from Urban–Suburban Observations in Chongqing, China

Yimei Wang [a, b, ★], Junjie Ding [a, b, c, ★], Jie Zhao [a, b], Peng Zhang [a, c], Jun Chen [a], Wei Huang [a, c], Xin Zhang [a, b], Xi Pu [a, c], Mengyao Wang [a, c], Pengrui Fu [a], Jiayan Yu [a, b, c *]

Correspondence to: Jiayan Yu (jiayan.yu@klapc.org.cn)

Table S1. The comparison of BC concentrations (unit: μg·m^{-3}) in megacities worldwide.

Country	Sampling location	Site type	Sampling preiod	Equipment	BC±1SD (μg·m^{-3})	Reference
Italy	Milan	Urban	Jul 2017 to Mar 2018	AE31	1.921±0.876	[1]
		Suburban	Jul 2017 to Mar 2018	AE51	2.763±1.05	
UK	London	Urban	Jan 2013 to Apr 2015	AE22	6.6	[2]
		Suburban	Jan 2013 to Apr 2015	MAAP	1.2	
Spain	Madrid	Urban	Dec 2014 to Nov 2015	AE33	3.70±3.73	[3]
		Urban	Dec 2014 to Nov 2015	AE33	2.33±2.96	
		Suburban	Dec 2014 to Nov 2015	AE33	2.61±5.04	
France	Paris	Urban	Dec 2017 to 2019	AE33	2.5±1.7	[4]
		Suburban	Dec 2017 to 2019	AE33	1.8±2.4	
USA	New york	Urban	May 2003 to Dec 2003	AE21	2.04	[5]
		Urban	2004 annual	AE21	1.99	
		Urban	2005 annual	AE21	1.72	
		Urban	2006 annual	AE21	1.69	
		Urban	2007 annual	AE21	1.67	
		Urban	2008 annual	AE21	1.71	
		Urban	2009 annual	AE21	1.81	
		Urban	2010 annual	AE21	1.61	
		Urban	2011 annual	AE21	1.7	

		Urban	2012 annual	AE21	1.39	
		Suburban	May 2004 to Dec 2004	AE21	0.7	
		Suburban	2005 annual	AE21	0.76	
		Suburban	2006 annual	AE21	0.71	
		Suburban	2007 annual	AE21	0.72	
		Suburban	2008 annual	AE21	0.67	
		Suburban	2009 annual	AE21	0.57	
		Suburban	2010 annual	AE21	0.46	
		Suburban	2011 annual	AE21	0.58	
		Suburban	2012 annual	AE21	0.57	
	Los Angeles	Urban	Mar 2016 to Feb 2017	AE33	0.64	6
		Suburban	Mar 2016 to Feb 2017	AE33	1.04	
Mexico	Mexico city	Urban	2015 annual	AE33	2.52	7
		Suburban	2015 annual	AE33	0.75	
		Urban	Apr 2016 to Mar 2017	TOT/TOR	1.18	8
Japan	Tokyo	Urban	Apr 2016 to Mar 2017	TOT/TOR	0.66	
		Suburban	Apr 2016 to Mar 2017	TOT/TOR	1.59	
India	Delhi	Suburban	Apr 2015 to Mar 2016	AE33	7.2 ± 0.3	9
		Urban	Apr 2016 to Feb 2017	AE51	21.33	10
	Shanghai	Urban	Jun 2016 to Jun 2017	AE31	1.17± 0.61	11
		Suburban	Jun 2016 to Jun 2017	AE31	2.09± 0.97	
China		Suburban	2013 annual	OR	6.42±4.35	12
	Beijing	Suburban	2014 annual	OR	7.86±4.71	
		Suburban	2015 annual	OR	6.58±4.22	
		Suburban	2016 annual	OR	5.91±3.51	

	Suburban	2017 annual	OR	5.28±3.11	
	Suburban	2018 annual	OR	4.59±2.78	
	Suburban	2019 annual	OR	3.7±2.22	
	Urban	2012 annual	AE22	6.25±5.73	[13]
	Urban	2013 annual	AE22	5.8±5.5	
	Urban	2014 annual	AE22	5.5±5.4	
	Urban	2015 annual	AE22	4.6±4.9	
	Urban	2016 annual	AE22	3.9±4.2	
	Urban	2017 annual	AE22	3.1±3.5	
	Urban	2018 annual	AE22	2.4±3.1	
	Urban	2019 annual	AE22	2±2.8	
	Urban	2020 annual	AE22	1.8±1.54	
Guangzhou	Urban	Dec 2020 to Sep 2021	TOT	1.32 ± 0.77	[14]
	Suburban	Dec 2020 to Sep 2021	TOT	1.12 ± 0.44	
Shenzhen	Urban	Jan 2014 to Jun 2015	AE31	2.58±1.91	[15]
	Suburban	Jan 2014 to Jun 2015	AE31	1.12±0.90	
Chongqing	Suburban	2024 annual	AE33	2.83 ± 1.85	This study
	Urban	2024 annual	AE33	2.39 ± 1.31	

AE: Aethalometer; MAAP: Multi Angle Absorption Photometer; COSMOS: Continuous Soot Monitoring System; SP2: Single Particle Soot Photometer; TOT: Thermal-Optical Transmittance method; OR: Optical Reflectance method.

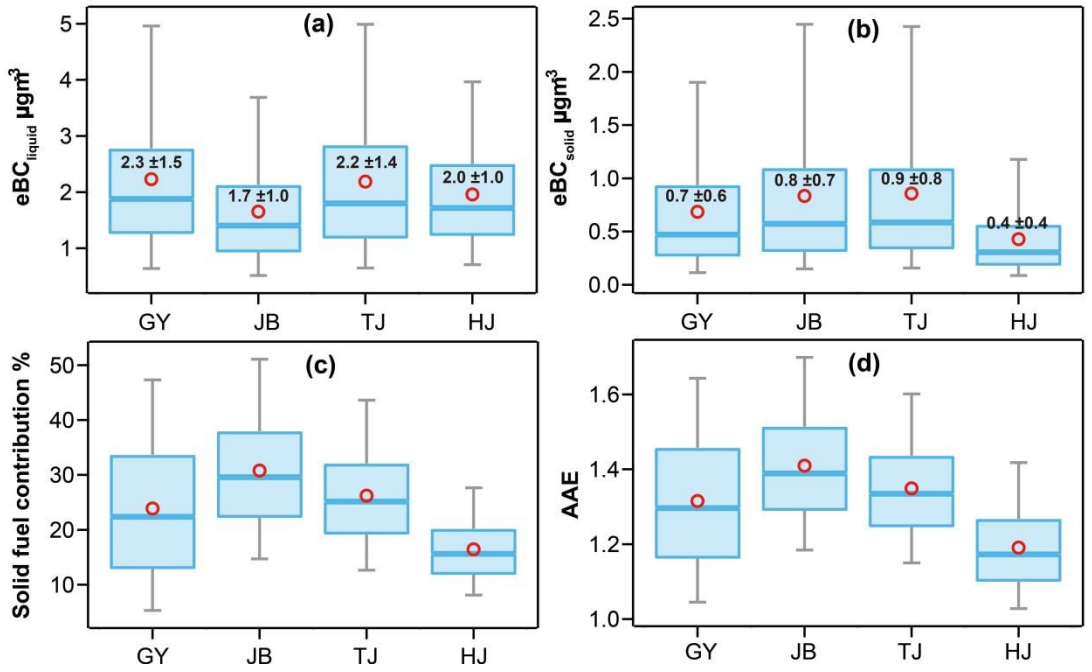

Fig. S1. Box plots of eBC_{liquid}, eBC_{solid}, solid fuel contribution, and AAE at four sites during the sampling period.

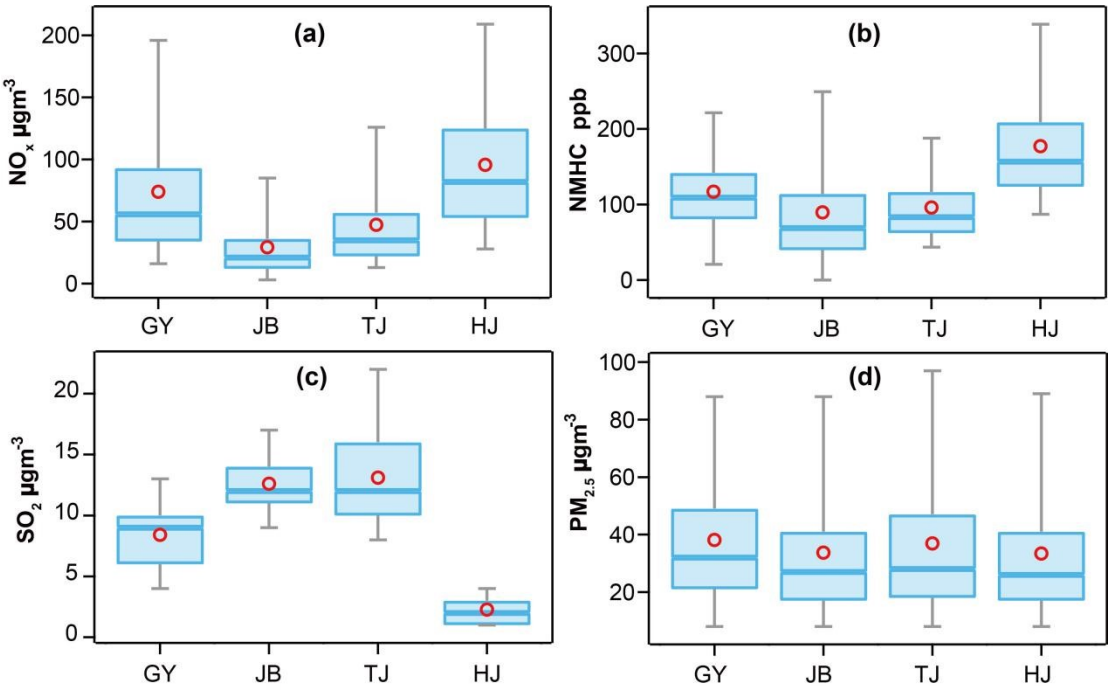

Fig. S2. Box plots of NO_x, NMHC, SO_2, and $PM_{2.5}$ at four sites during the sampling period.

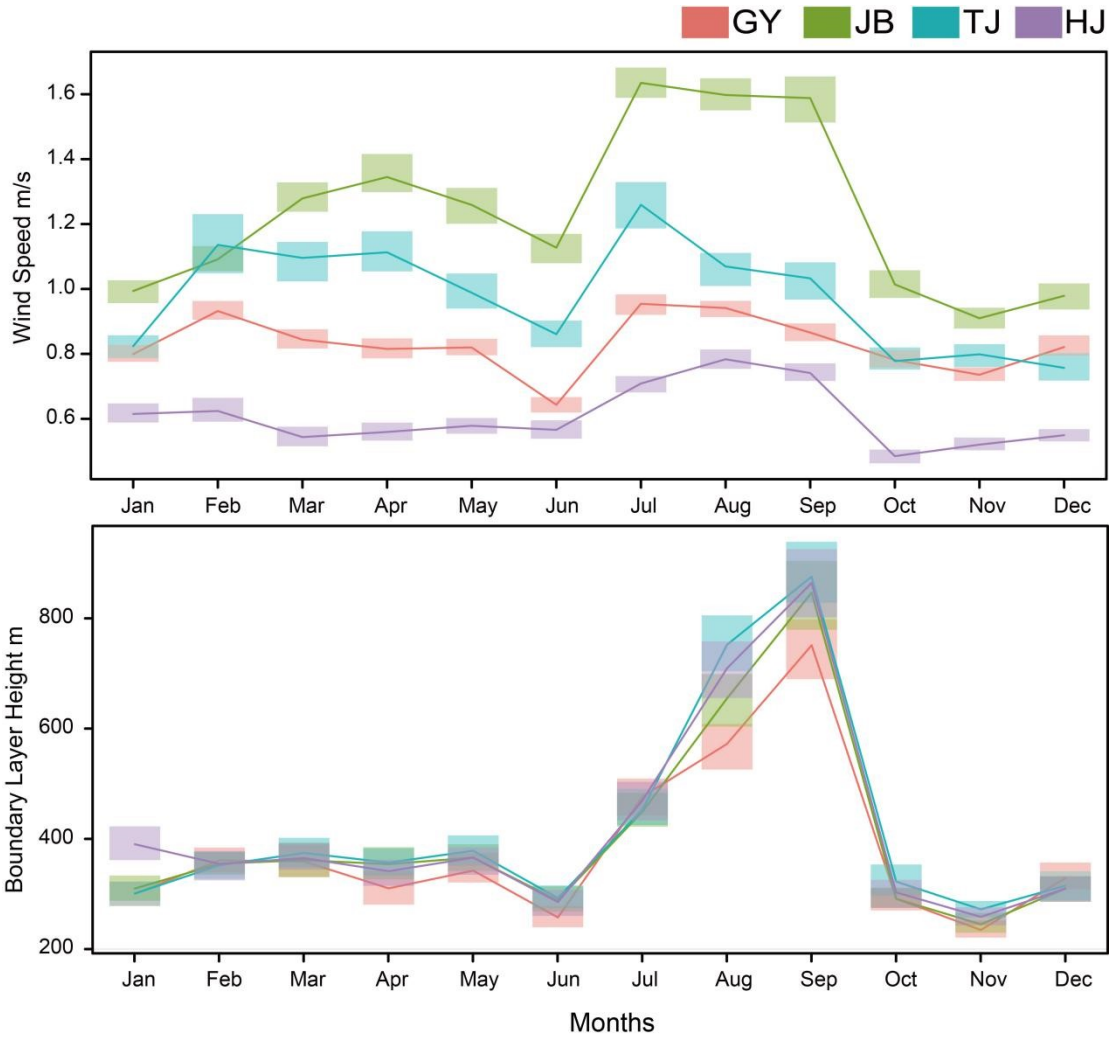

Fig. S3. Box plots of monthly variations in Wind speed (WS) and boundary layer height (BLH) across the sites.

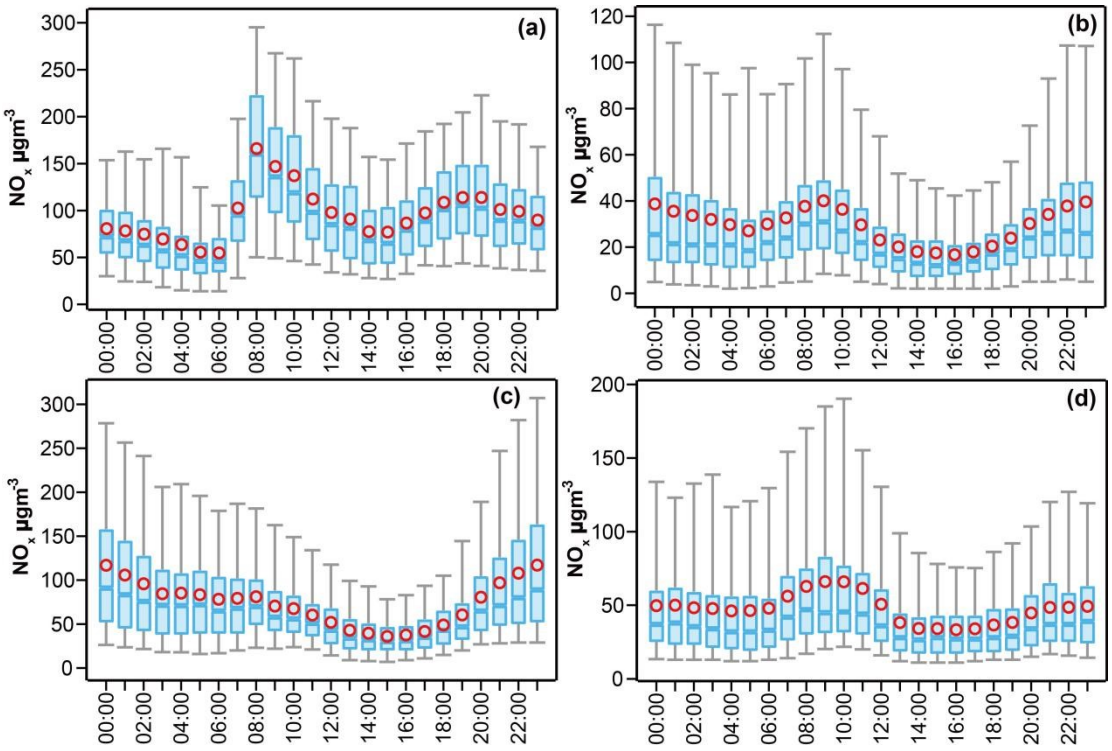

Fig. S4. Mean hourly NO_x concentrations at (a) HJ, (b) JB, (c) GY, and (d) TJ sites.

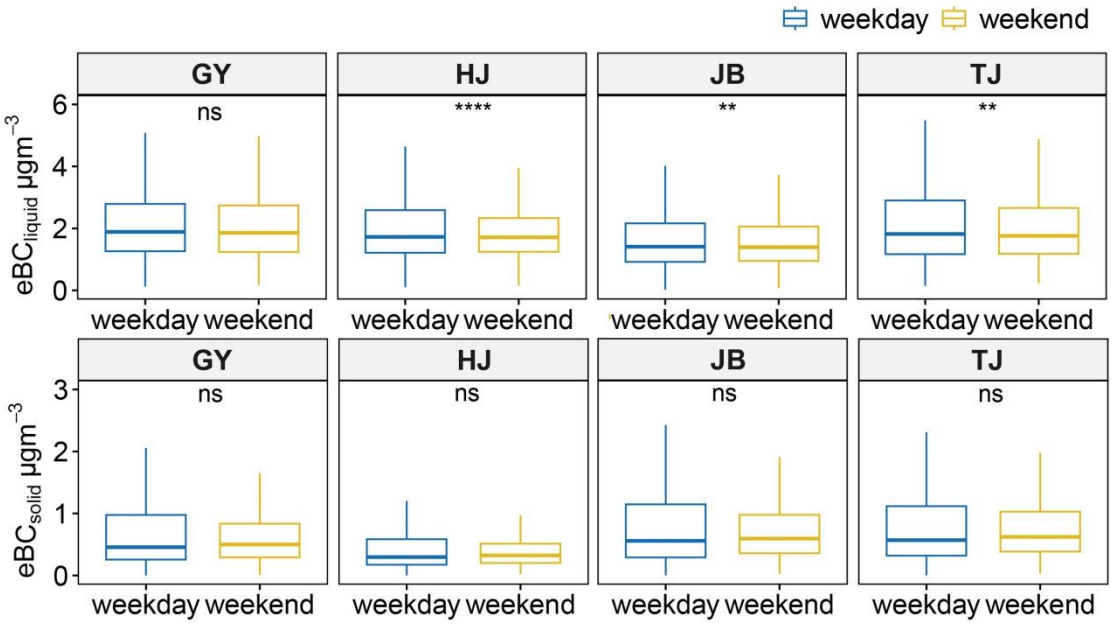

Fig. S5. Statistical results of eBC_{liquid} and eBC_{solid} from the independent samples t-test comparing weekday and weekend data. The blue box plot represents weekday data, while the yellow box plot represents weekend data.

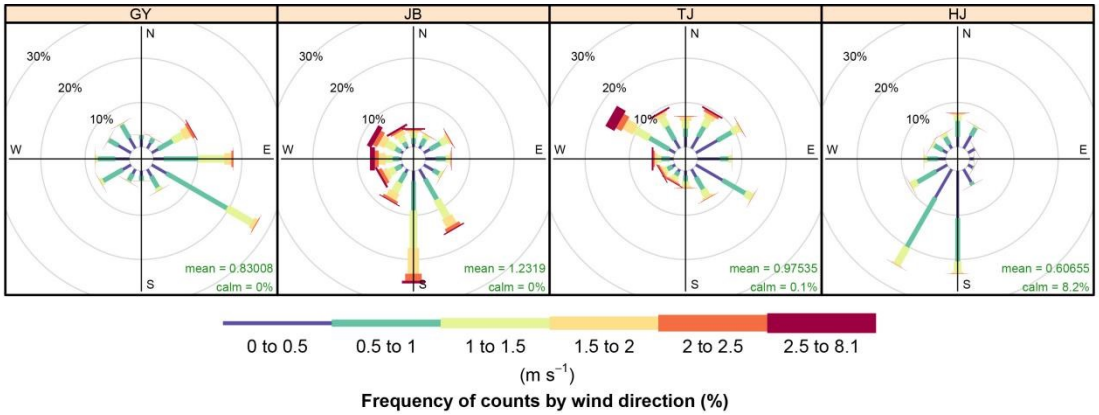

Fig. S6. Wind rose diagrams for four sites, showing the distribution of wind direction and speed during the sampling period.

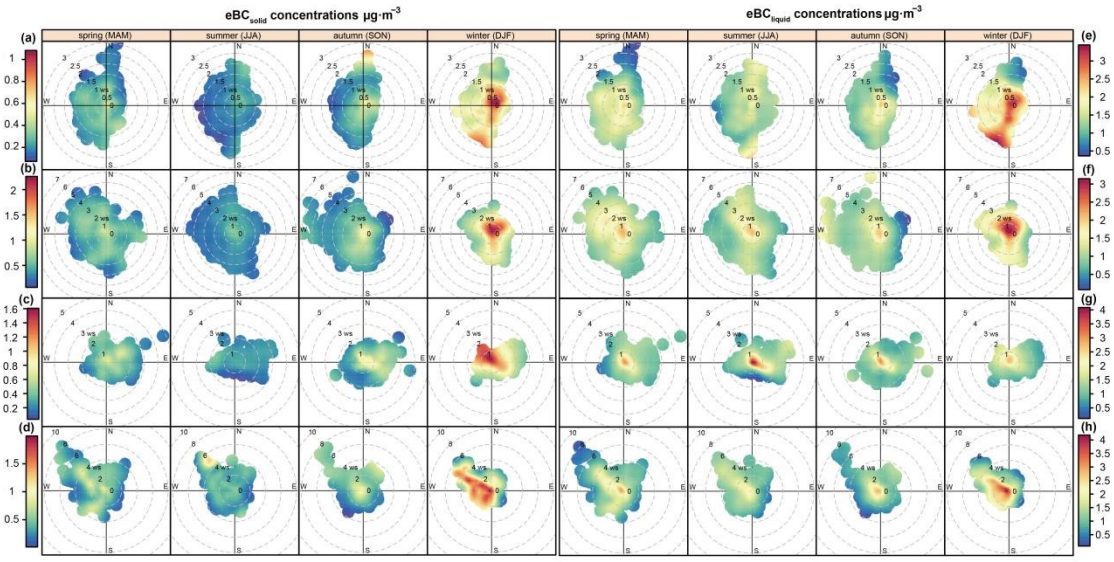

Fig. S7. Polar plots of eBC_{solid} and eBC_{liquid} for seasonal variations at all sites. (a) eBC_{solid} at HJ, (b) eBC_{solid} at JB, (c) eBC_{solid} at GY, (d) eBC_{solid} at TJ, (e) eBC_{liquid} at HJ, (f) eBC_{liquid} at JB, (g) eBC_{liquid} at GY, and (h) eBC_{liquid} at TJ.

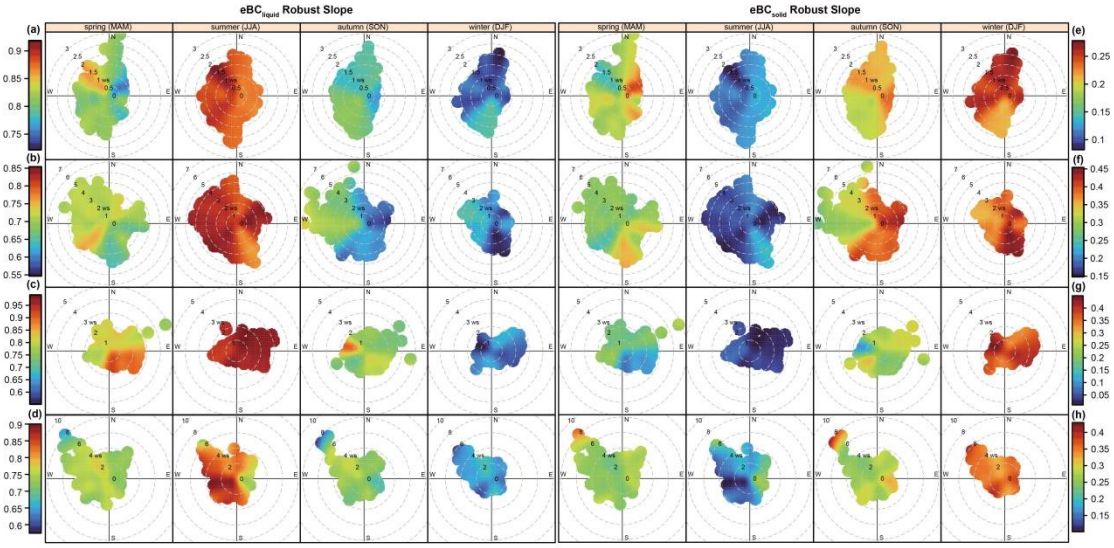

Fig. S8. Polar plots of the robust regression slope between eBC_{liquid} and eBC, and between eBC_{solid} and eBC for seasonal variations at all sites. (a) eBC_{liquid} at HJ, (b) eBC_{liquid} at JB, (c) eBC_{liquid} at GY, (d) eBC_{liquid} at TJ, (e) eBC_{solid} at HJ, (f) eBC_{solid} at JB, (g) eBC_{solid} at GY, and (h) eBC_{solid} at TJ.

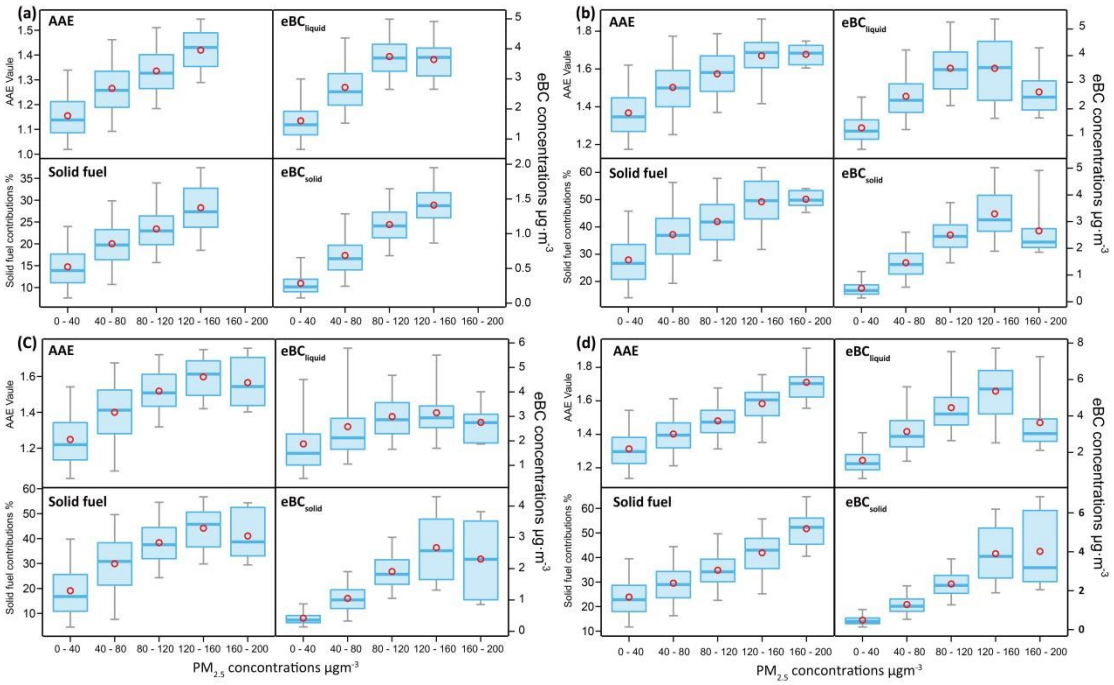

Fig. S9. Box plots of AAE, eBC_{liquid}, solid fuel contribution, and eBC_{solid} as a function of $PM_{2.5}$ concentration at (a) HJ, (b) JB, (c) GY, and (d) TJ sites.

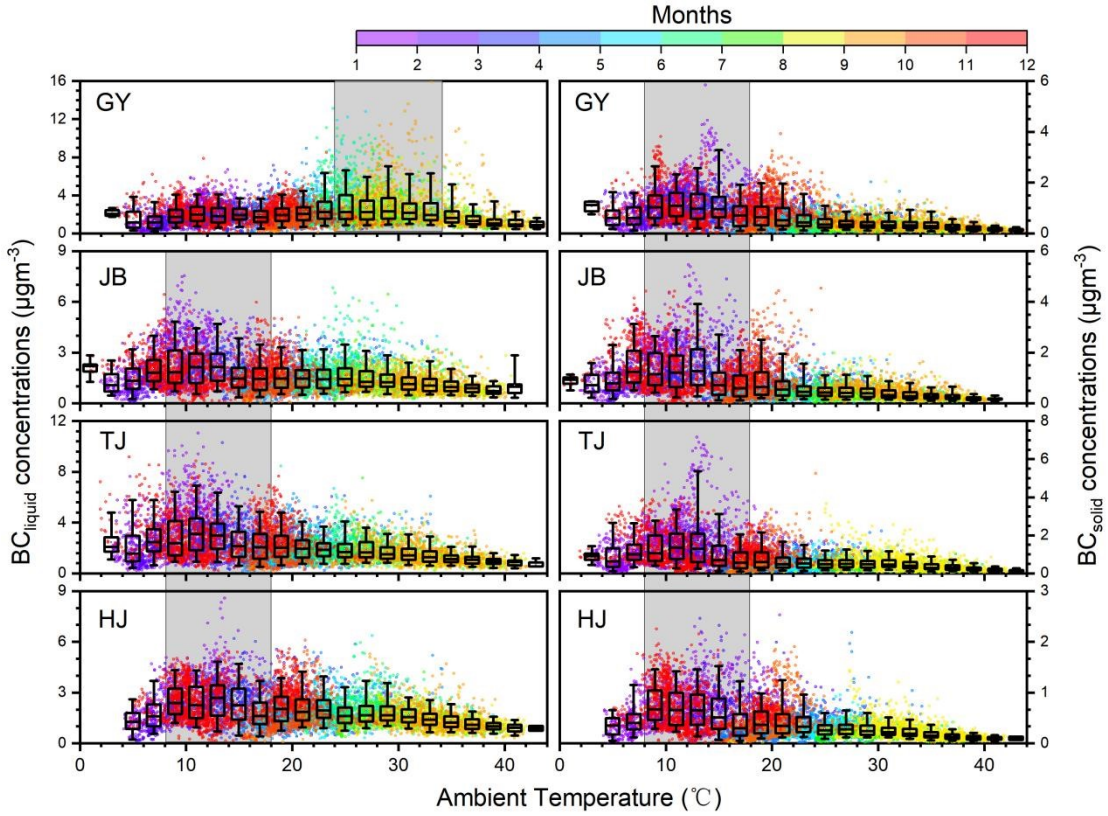

Fig. S10. Scatter plots and box plots of eBC concentration as a function of temperature across the sites.

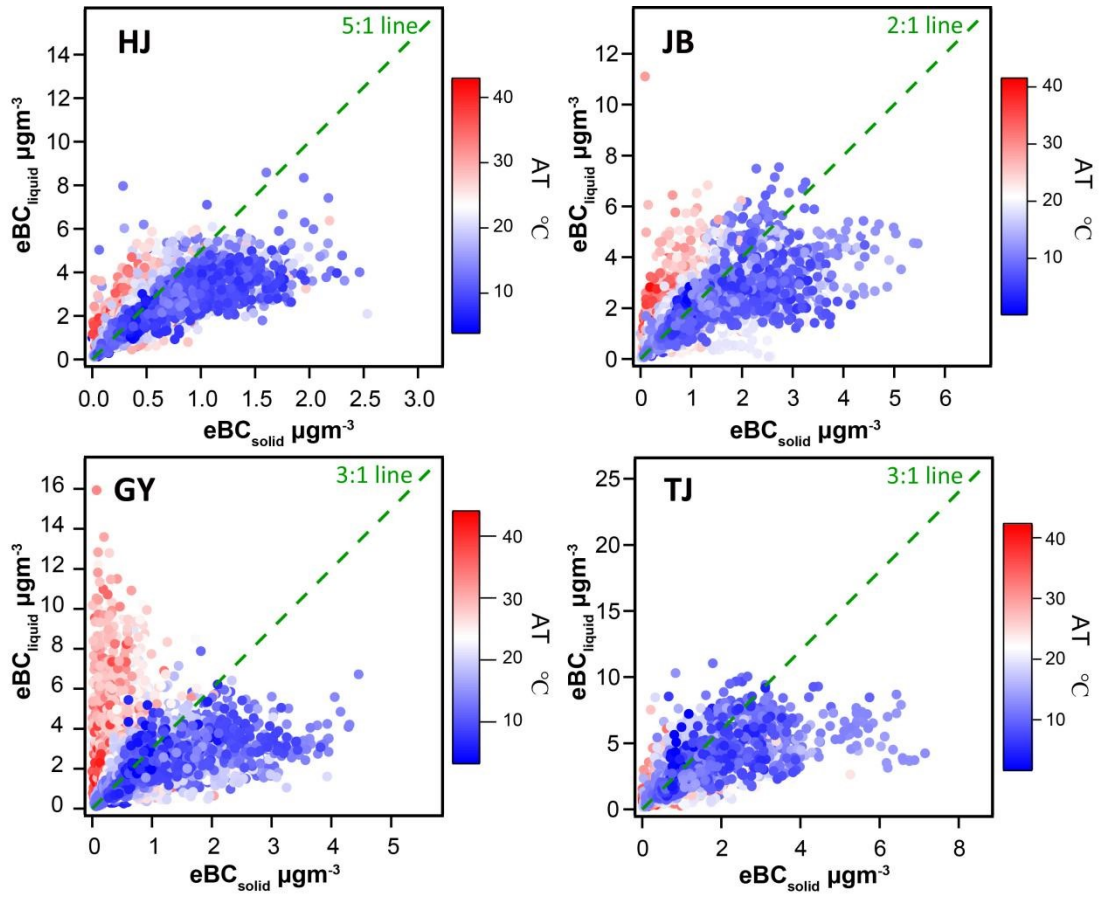

Fig. S11. Temperature dependence of eBC_{liquid} and eBC_{solid} at each site.

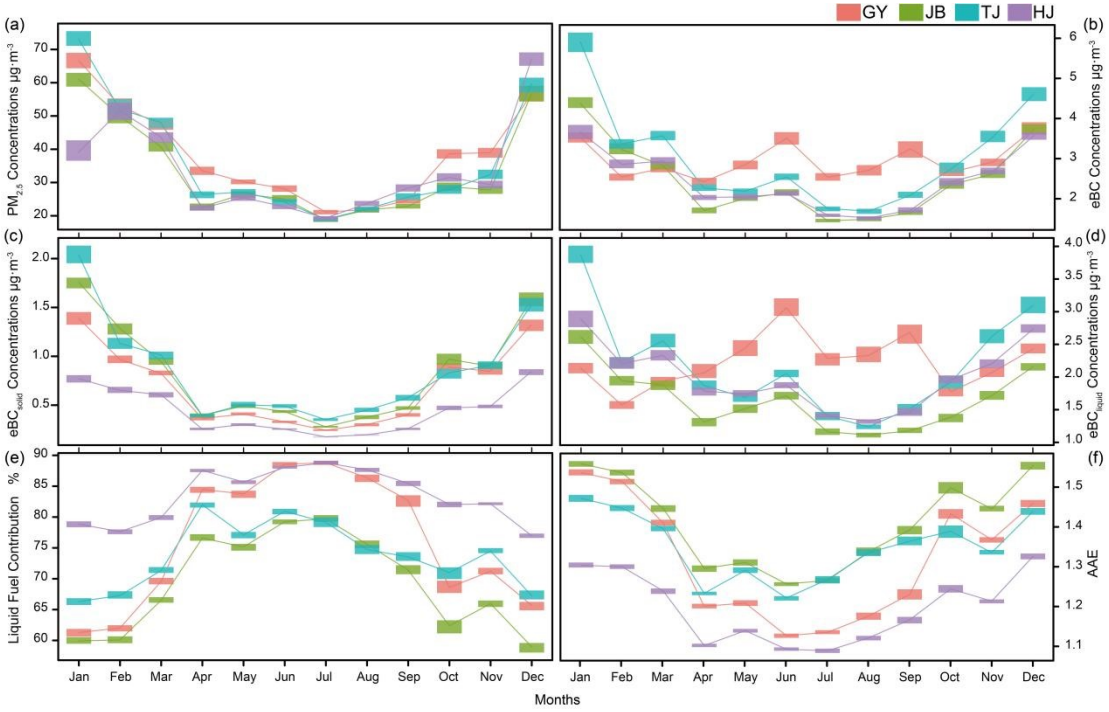

Fig. S12. Box plots of monthly varations in (a) $PM_{2.5}$, (b) eBC_{total}, (c) eBC_{solid}, (d) eBC_{liquid}, (e) liquid fuel contribution, and (f) AAE across the sites.

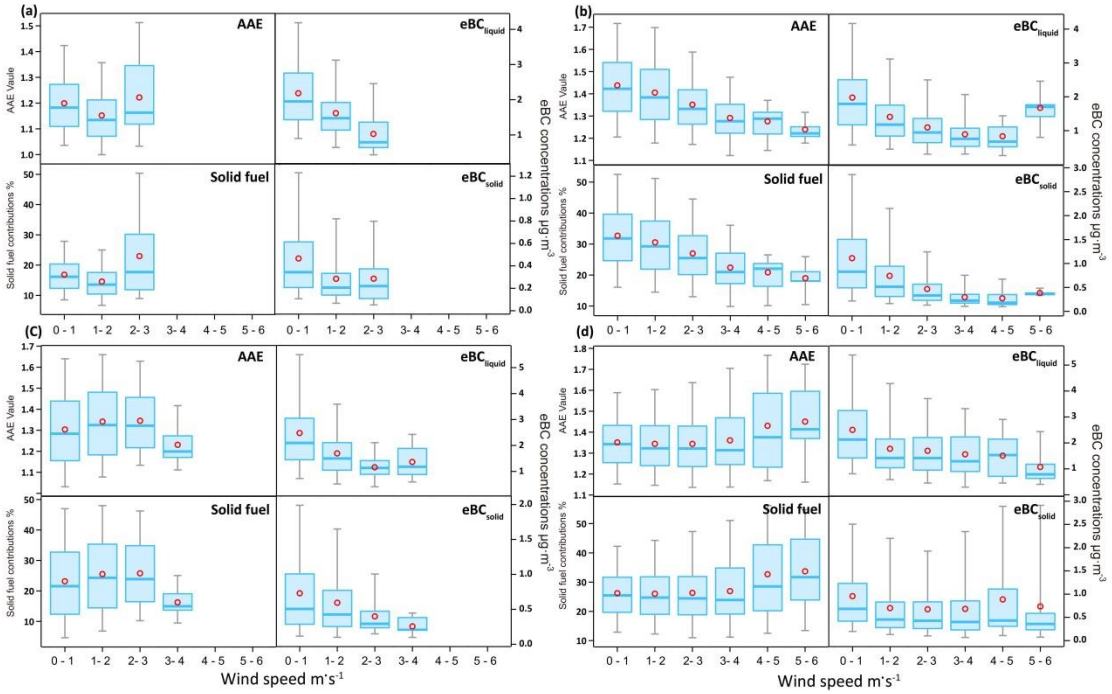

Fig. S13. Box plots of AAE, eBC_{liquid}, solid fuel contribution, and eBC_{solid} as a function of wind speed at (a) HJ, (b) JB, (c) GY, and (d) TJ sites.

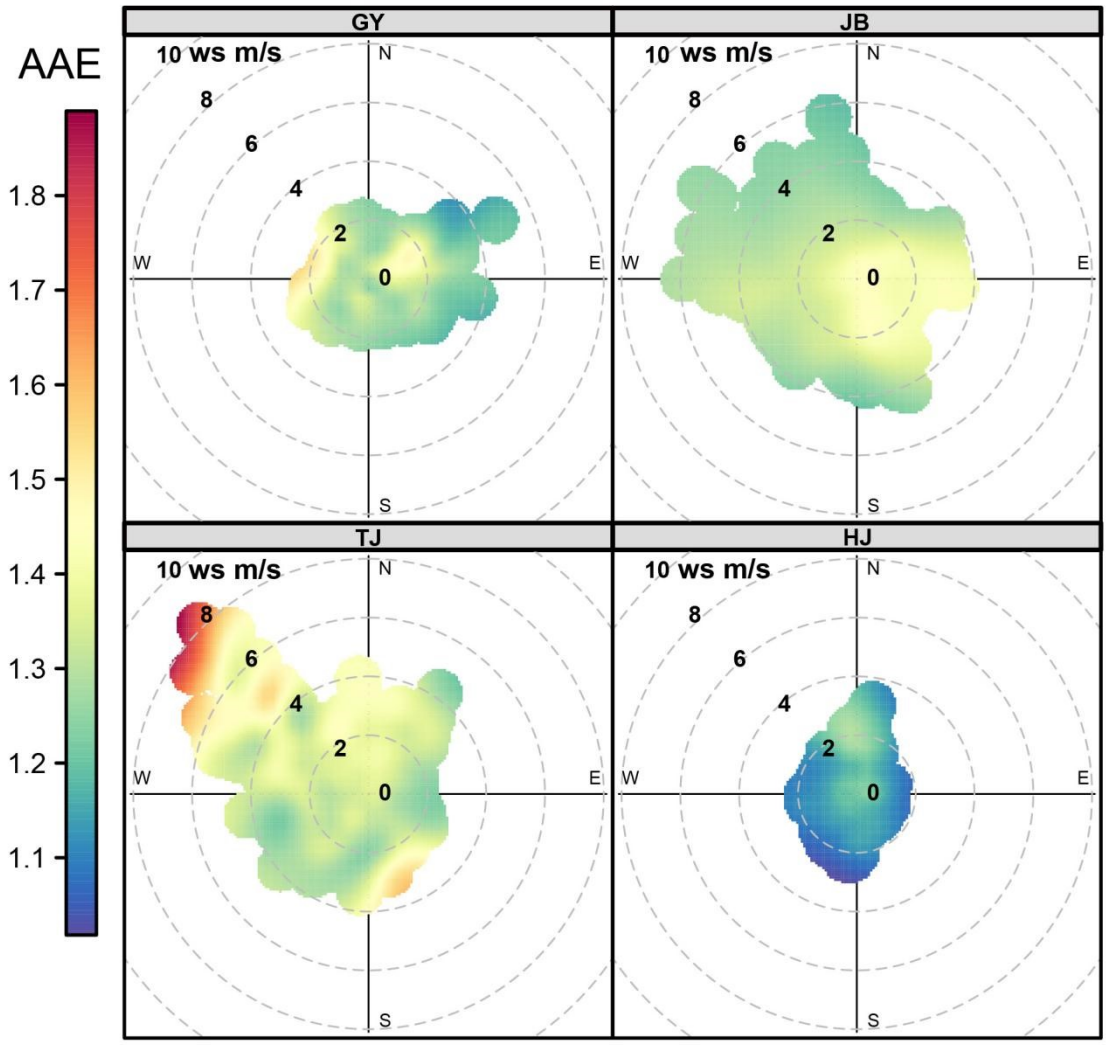

Fig. S14. Polar plots of AAE at each sites.

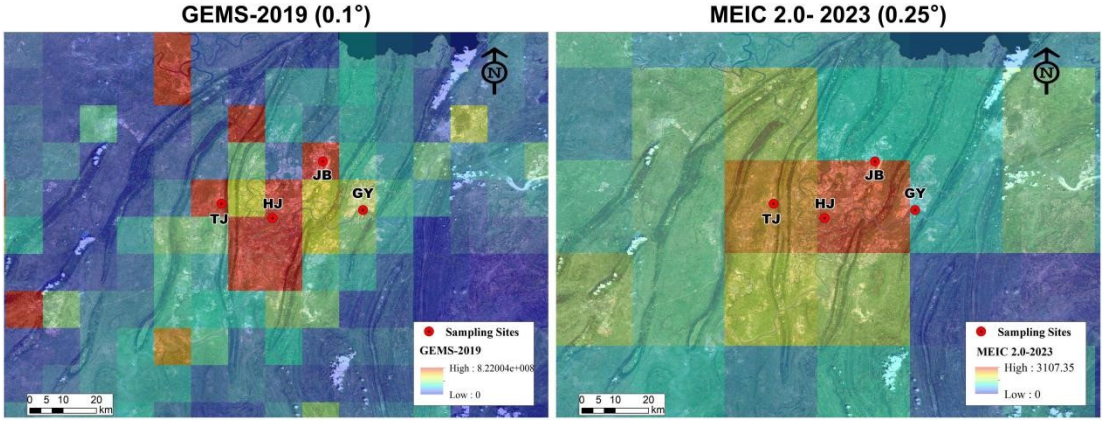

Fig. S15. Comparison of gridded BC emissions over the study region from GEMS (2019, 0.1° × 0.1°) and MEIC v2.0 (2023, 0.25° × 0.25°).

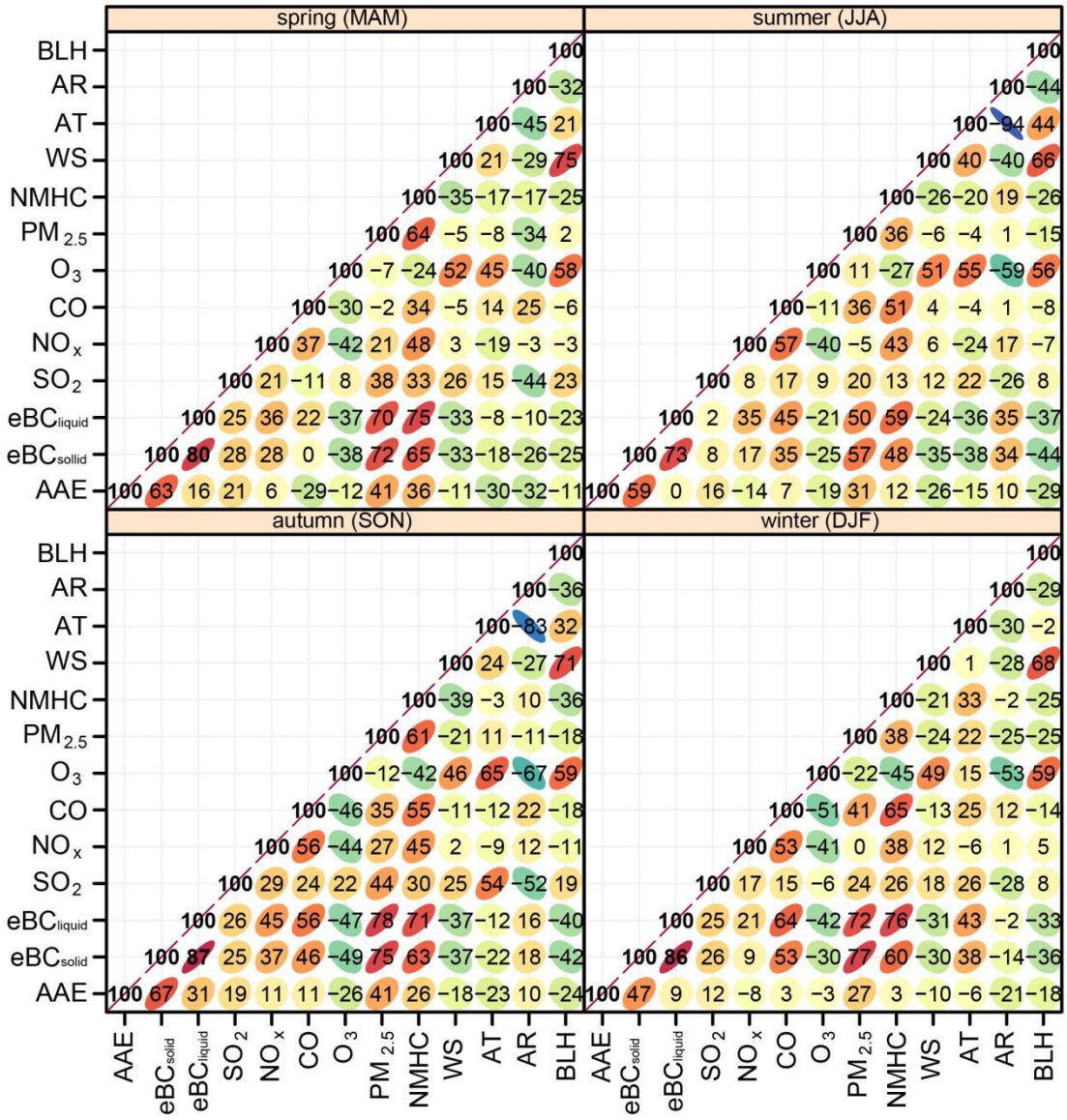

Fig. S16. Seasonal correlation matrices between the pollutants at the HJ site.

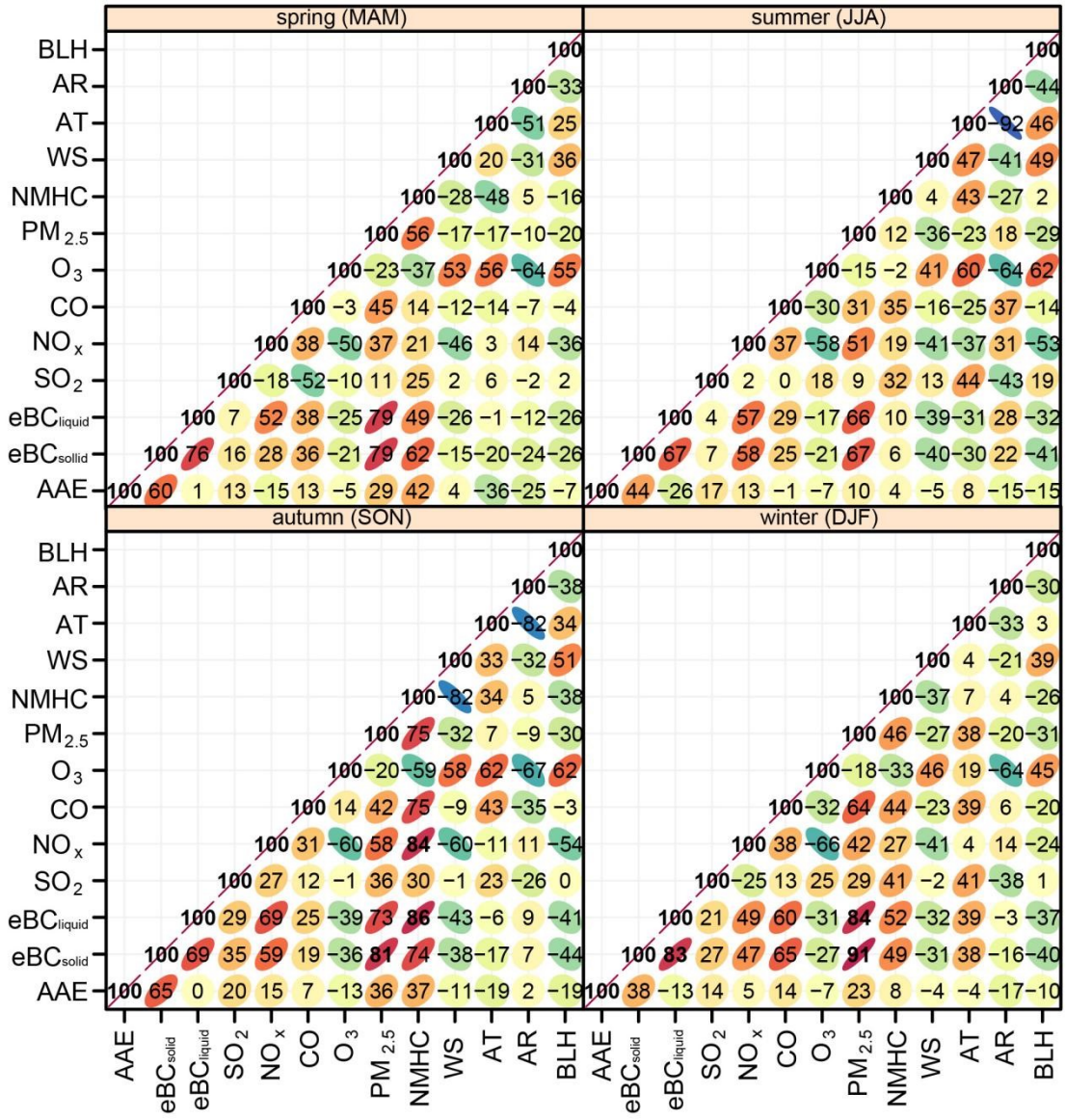

Fig. S17. Seasonal correlation matrices between the pollutants at the JB site.

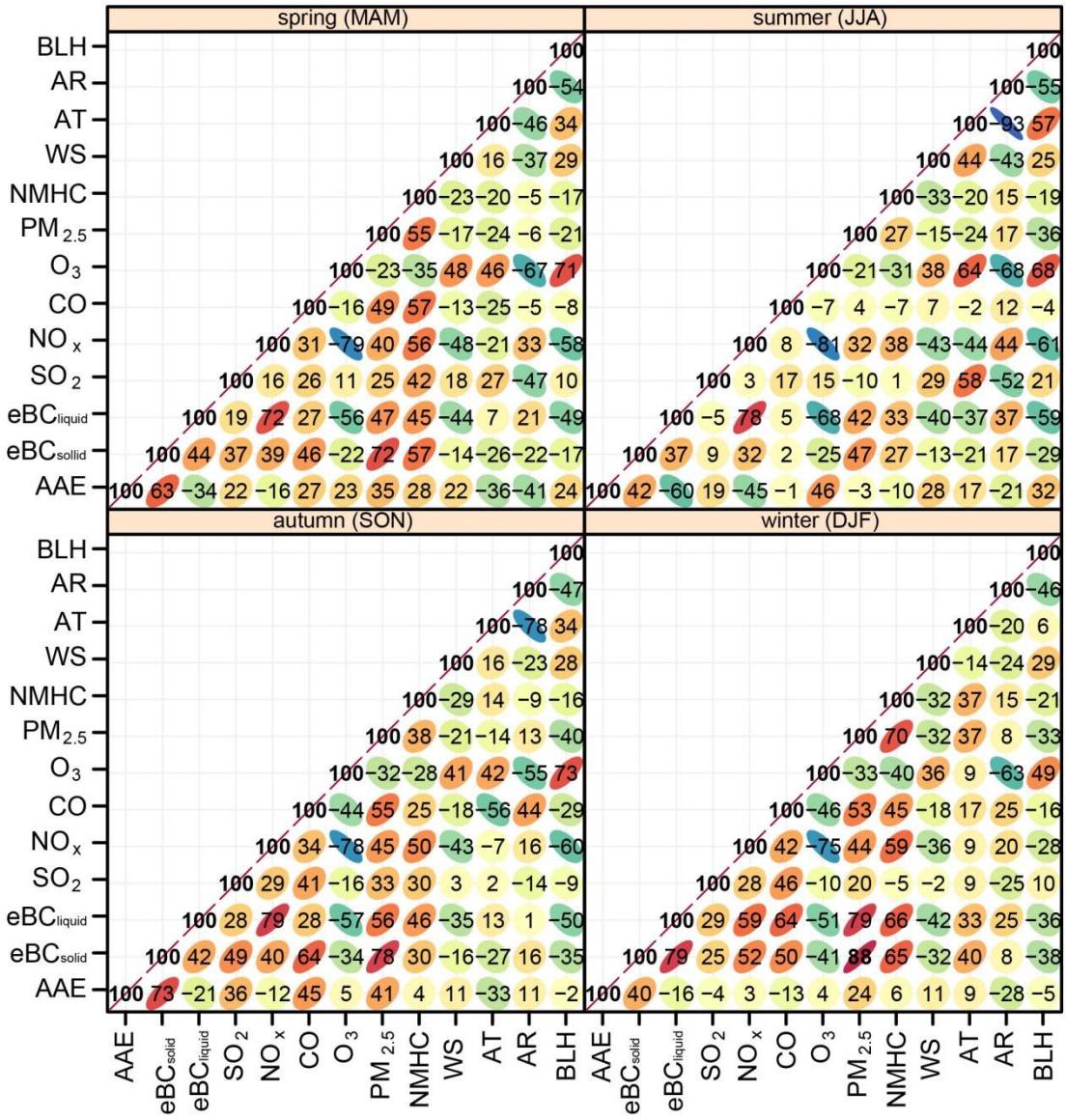

Fig. S18. Seasonal correlation matrices between the pollutants at the GY site.

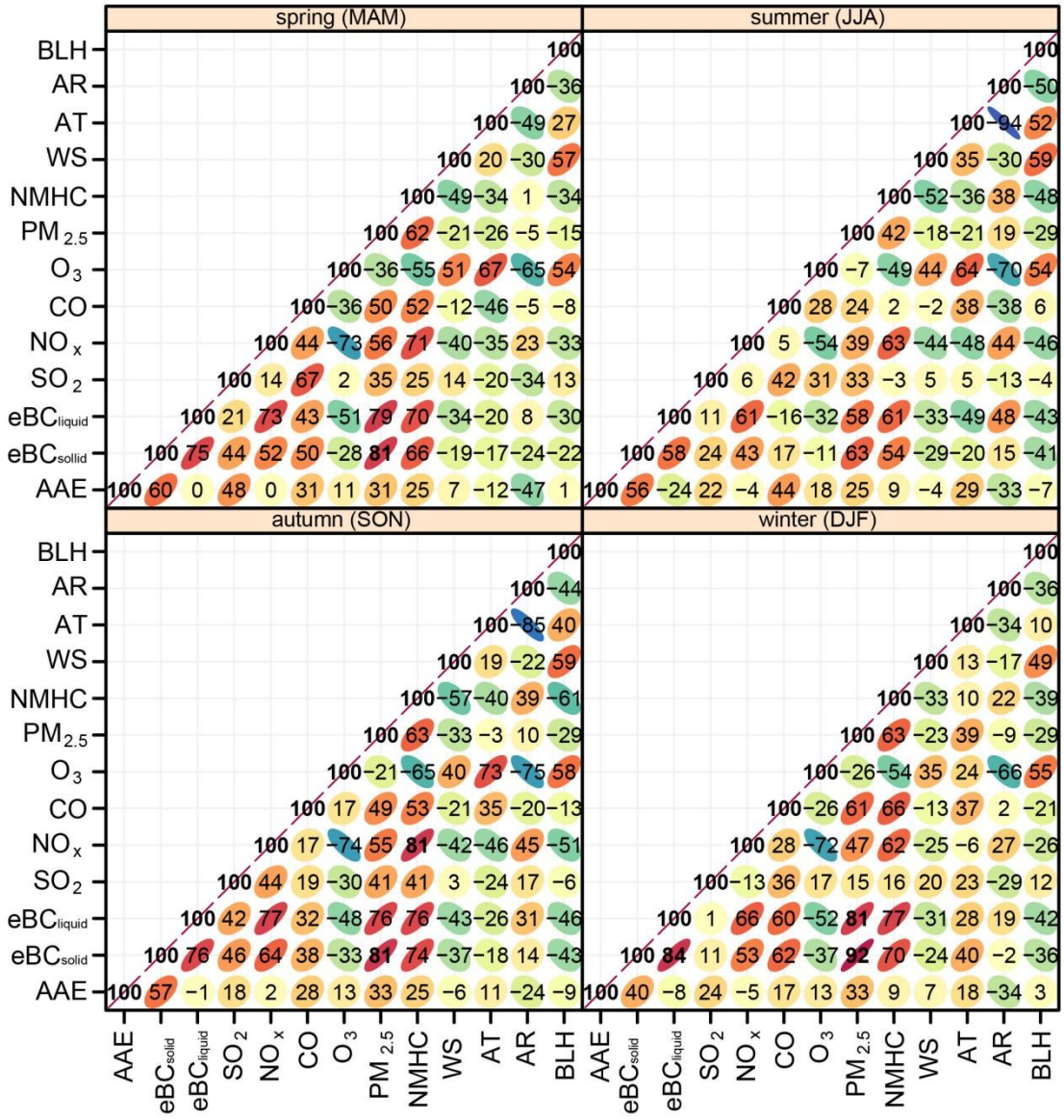

Fig. S19. Seasonal correlation matrices between the pollutants at the TJ site.

Table S2. GuoYuan Port Cargo Throughput rencently (unit: Million Tons, Mt).

Time period	Cargo throughput	Reference
Jan to Nov 2024	26.006 Mt	https://www.cq.gov.cn/zt/xblhxtd/rdxw/202412/t20241218_13902977.html
Jan to Jun 2024	12.909 Mt	https://jtj.cq.gov.cn/sy_240/bmdt/202407/t20240

		718_13381096.html
Jul to Nov 2024	2.619 Mt per month	derived from above data
Jan to Jun 2024	2.151 Mt per month	derived from above data
Jan-25	2.146 Mt	https://www.cqgyzone.com/home/articles/1379.html
Jan to Mar 2025	2.214 Mt per month	https://jtj.cq.gov.cn/sy_240/bmdt/202504/t20250411_14514839.html

References

1 A. Mousavi, M. H. Sowlat, C. Lovett, M. Rauber, S. Szidat, R. Boffi, A. Borgini, C. De Marco, A. A. Ruprecht and C. Sioutas, Source apportionment of black carbon (BC) from fossil fuel and biomass burning in metropolitan Milan, Italy, *Atmospheric Environment*, 2019, **203**, 252–261.

2 K. P. Wyche, R. L. Cordell, L. Smith M, K. L. Smallbone, P. Lyons, S. M. L. Hama, P. S. Monks, J. Staelens, J. Hofman, C. Stroobants, E. Roekens, G. P. A. Kos, E. P. Weijers, P. Panteliadis and M. B. A. Dijkema, The spatio-temporal evolution of black carbon in the North-West European 'air pollution hotspot', *Atmospheric Environment*, 2020, **243**, 117874.

3 M. Becerril-Valle, E. Coz, A. S. H. Prévôt, G. Močnik, S. N. Pandis, A. M. Sánchez De La Campa, A. Alastuey, E. Díaz, R. M. Pérez and B. Artíñano, Characterization of atmospheric black carbon and co-pollutants in urban and rural areas of Spain, *Atmospheric Environment*, 2017, **169**, 36–53.

4 M. Savadkoohi, M. Pandolfi, C. Reche, J. V. Niemi, D. Mooibroek, G. Titos, D. C. Green, A. H. Tremper, C. Hueglin, E. Liakakou, N. Mihalopoulos, I. Stavroulas, B. Artiñano, E. Coz, L. Alados-Arboledas, D. Beddows, V. Riffault, J. F. De Brito, S. Bastian, A. Baudic, C. Colombi, F. Costabile, B. Chazeau, N. Marchand, J. L. Gómez-Amo, V. Estellés, V. Matos, E. Van Der Gaag, G. Gille, K. Luoma, H. E. Manninen, M. Norman, S. Silvergren, J.-E. Petit, J.-P. Putaud, O. V. Rattigan, H. Timonen, T. Tuch, M. Merkel, K. Weinhold, S. Vratolis, J. Vasilescu, O. Favez, R. M. Harrison, P. Laj, A. Wiedensohler, P. K. Hopke, T. Petäjä, A. Alastuey and X. Querol, The variability of mass concentrations and source apportionment analysis of equivalent black carbon across urban Europe, *Environment International*, 2023, **178**, 108081.

5 O. V. Rattigan, K. Civerolo, P. Doraiswamy, H. D. Felton and P. K. Hopke, Long Term Black Carbon Measurements at Two Urban Locations in New York, *Aerosol Air Qual. Res.*, 2013, **13**, 1181–1196.
6 A. Mousavi, M. H. Sowlat, S. Hasheminassab, A. Polidori and C. Sioutas, Spatio-temporal trends and source apportionment of fossil fuel and biomass burning black carbon (BC) in the Los Angeles Basin, *Science of The Total Environment*, 2018, **640–641**, 1231–1240.
7 O. Peralta, A. Ortínez-Alvarez, R. Basaldud, N. Santiago, H. Alvarez-Ospina, K. De La Cruz, V. Barrera, M. De La Luz Espinosa, I. Saavedra, T. Castro, A. Martínez-Arroyo, V. H. Páramo, L. G. Ruíz-Suárez, F. A. Vazquez-Galvez and A. Gavilán, Atmospheric black carbon concentrations in Mexico, *Atmospheric Research*, 2019, **230**, 104626.
8 H. Hayami, S. Saito and S. Hasegawa, Spatiotemporal Variations of Fine Particulate Organic and Elemental Carbons in Greater Tokyo, *Asian J. Atmos. Environ*, 2019, **13**, 161–170.
9 U. C. Dumka, D. G. Kaskaoutis, S. Tiwari, P. D. Safai, S. D. Attri, V. K. Soni, N. Singh and N. Mihalopoulos, Assessment of biomass burning and fossil fuel contribution to black carbon concentrations in Delhi during winter, *Atmospheric Environment*, 2018, **194**, 93–109.
10 U. C. Dumka, D. G. Kaskaoutis, P. C. S. Devara, R. Kumar, S. Kumar, S. Tiwari, E. Gerasopoulos and N. Mihalopoulos, Year-long variability of the fossil fuel and wood burning black carbon components at a rural site in southern Delhi outskirts, *Atmospheric Research*, 2019, **216**, 11–25.
11 X. Peng, M. Liu, Y. Zhang, Z. Meng, V. Achal, T. Zhou, L. Long and Q. She, The characteristics and local-regional contributions of atmospheric black carbon over urban and suburban locations in Shanghai, China, *Environmental Pollution*, 2019, **255**, 113188.
12 J. Zhang, Y. Yao, C. Xiao, Y. Gu, X. Jin, P. Wang and L. Zhao, The pollution characterization of black carbon aerosols in the southwest suburb of beijing from 2013 to 2019, *Atmospheric Pollution Research*, 2023, **14**, 101669.
13 J. Sun, Z. Wang, W. Zhou, C. Xie, C. Wu, C. Chen, T. Han, Q. Wang, Z. Li, J. Li, P. Fu, Z. Wang and Y. Sun, Measurement report: Long-term changes in black carbon and aerosol optical properties from 2012 to 2020 in Beijing, China, *Atmospheric Chemistry and Physics*, 2022, **22**, 561–575.
14 J. Su, R. Zhang, B. Liu, M. Tong, S. Xiao, X. Wang, Q. Zhao, W. Song, D. Talifu and X. Wang, Seasonal and Day–Night Variations in Carbonaceous Aerosols and Their Light-Absorbing Properties in Guangzhou, China, *Atmosphere*, 2023, **14**, 1545.
15 D. Cheng, C. Wu, L. Song, T. L. Sun and A. M. Liu, Comparative study on the characteristics of black carbon aerosol in urban and suburban areas of Shenzhen, *China Environ. Sci.*, 2018, **38**, 1653–1662.